DOI: 10.1002/((please add manuscript number))

Article type: Communication

"Self-matched" Tribo-/Piezoelectric Nanogenerators Using Vapor-induced Phase-separated Polyvinylidene Fluoride and Recombinant Spider Silk

Tao Huang[†], Yujia Zhang[†], Peng He, Gang Wang, Xiaoxia Xia, Guqiao Ding[*] and Tiger H. Tao[*]

T. Huang, Y. Zhang, Dr. P. He, Dr. G. Wang, Prof. G. Q. Ding, Prof. T. H. Tao

Shanghai Institute of Microsystem and Information Technology, Chinese Academy of Sciences, Shanghai 200050, P. R. China.

Email: tiger@mail.sim.ac.cn; gqding@mail.sim.ac.cn

College of Materials Science and Opto-Electronic Technology, University of Chinese Academy of Sciences, Beijing, 100049, P. R. China.

Prof. X. Xia

State Key Laboratory of Microbial Metabolism, School of Life Sciences and Biotechnology, Shanghai Jiao Tong University, Shanghai 200240, China

Prof. T. H. Tao

School of Physical Science and Technology, ShanghaiTech University, Shanghai 200031, China

Institute of Brain-Intelligence Technology, Zhangjiang Laboratory, Shanghai 200031, China

Shanghai Research Center for Brain Science and Brain-Inspired Intelligence, Shanghai 200031, China

Keywords: tribo-/piezoelectric nanogenerator, spider silk, vapor-induced phase-separation, implantable energy harvester

Abstract:

Flexible biocompatible mechanical energy harvesters are drawing increasing interest because of their high energy harvesting efficiency for powering wearable/implantable devices. Here we report a type of "self-matched" tribo-piezoelectric nanogenerators composed of genetically engineered recombinant spider silk protein and piezoelectric polyvinylidene fluoride (PVDF)-decorated polyethylene terephthalate (PET) layers. The PET layer serves as a shared structure and electrification layer for both piezoelectric and triboelectric nanogenerators. Importantly, the PVDF generates a strong piezo-potential which modifies the surface-potential of the PET layer to match the electron transferring direction of spider silk during triboelectrification. A "vapor-induced phase-separation" process is developed to enhance the piezoelectric performance in a facile and "green" roll-to-roll manufacturing fashion. Our devices show exceptional output performance and energy transformation efficiency among

currently existing energy harvesters of similar sizes and exhibit the potential for large-scale fabrication and various implantable/wearable applications.

Main Text

In the era of the Internet of Things (IoTs), sensors, portable electronics, wearable devices and wireless transport systems are increasing the demand for renewable and green energy supplies.[1,2] Triboelectric nanogenerators (TENGs) have been actively investigated and extensively developed, aiming for efficiently converting environmental mechanical energy into electricity for powering so-called self-powered sensors or systems.[3,4] However, some challenges, such as the large internal resistance, the low frictional efficiency, and material inefficiency for losing/gaining electrons, still remain to be overcome before current TENGs can be widely put into practical applications.[5] Recently, a modified concept, known as tribo-piezoelectric nanogenerators (TPNGs), offers an efficient approach to enhance the energy conversion efficiency.[6] This is because the thin-film structure of its active layers in both TENG and piezoelectric nanogenerator (PENG) allows facile integration into desired configurations for specific applications.[7-10]

Nevertheless, most TPNGs consisting of the tribo- and piezoelectric-components are based on direct energy superposition. The intrinsic electron-cloud-potential-well coupling effect of TENG is often overlooked.[11,12] It is known that the contact and separation of the two pairing tribo-materials generate

triboelectrification (or contact electrification). In this process, the charge transfer is affected by the relative capability of gaining or losing electrons, so called surface-potential difference, which intrinsically depends on the pairing materials themselves.[13] For example, silk proteins readily release electrons after contacting polyethylene terephthalate (PET) because of the huge surface-potential difference between silk and PET.[13] Nevertheless, a recent report shows that the spider silk protein can be genetically engineered to increase such potential difference with PET and be much easier to lose electrons than its natural counterparts.[14] However, for the paired PET and many other materials, there is a lack of effective methods to modify the surface potential.[15,16] Noticeably, piezoelectric materials can generate surface charge and electron potential under external forces because of the central symmetry breaking of the crystal structure.[17] Therefore, integrating the large surface charge generated by piezoelectric materials could be an effective way to modify the surface-potential difference of tribo-materials. Polyvinylidene fluoride (PVDF) is renowned as a good piezoelectric polymer material of simple fabrication and relatively low cost.[18,19] Furthermore, the excellent flexibility and biocompatibility make PVDF one of the most suitable materials to modify the surface potential of the triboelectric layer.[20]

Herein, we report a new approach in which the TENG and PENG are combined as an integrated device in a "self-matched" configuration to more efficiently harvest mechanical energy. Because of the surface-potential match, the piezoelectric effect in the PENG can induce a higher triboelectric output. Based on this approach, a set of self-matched TPNGs were fabricated using recombinant spider silk and PET/PVDF, demonstrating higher power output compared to existing hybrid devices in similar sizes. As innovations, we engineered the PVDF formation through a mild and "green" vapor-induced phase-separation process and introduced graphene to enhance the piezo-PVDF performance. Based on the highly polarized PVDF/graphene composite, the PET/PVDF-graphene was integrated with genetically engineered spider silk for "self-matched" energy harvesting. Furthermore, to explore the possibility of large-scale fabrication, we created a roll-to-roll method for the rapid and green preparation of our devices.

To illustrate the self-matching mechanism, we introduced the electron-cloud-potential-well model to explain the charge transfer between spider silk and PET, with or without PVDF enhancing, as shown in **Figure 1a**, where the detailed energy-band structure was simplified.[11] Here, the electrons occupying specific protein molecular orbits tend to transfer to the empty orbits of PET. Furthermore, the number of transferred electrons is proportional to the difference in potential-well depths between two materials (surface-potential difference). PVDF, a flexible piezoelectric and biocompatible polymer, has the capability to change the surface electron potential of the coupling material under mechanical

deformation. Therefore, we introduced PVDF to influence the surface potential of PET. The enhanced difference in potential wells depths between spider silk and PET/PVDF can significantly increase electron transfer thereby boosting energy output.

Based on this approach, the hybrid self-matched TPNG was fabricated as illustrated in **Figure 1b**. For the piezoelectric layer, a 10 wt.% PVDF/graphene (0.25% graphene content) solution in N, N′-dimethylformamide (DMF) was firstly spin-coated onto a PET substrate (thickness under 20 μm, see **Experimental Section**). Then, the spin-coated PET/PVDF was re-located to a humid environment for vapor-induced phase-separation processing (**Figure S1**), during which PVDF chains would be polarized in the direction from the substrate to humid air as shown in the grey dashed line box of **Figure 1b**.[21] Compared with electric-field polarization, metal ion doping and other reported methods, the vapor-induced phase-separation process is safer, more energy-saving and generates less pollution.[22,23] In addition, the *in situ* polarization of PVDF on PET substrates provided robust adhesion, directly obtaining the triboelectric layer. As reported recently, the deformations at the asperities via flexoelectric effect lead to more significant potential differences, which contributes to the higher voltage output.[24] As for the counter triboelectric layer, inkjet-print method was applied to coat the spider silk (~28.8 charge per chain) onto PET/ITO substrates with an average thickness of 2 μm similar control the surface asperities as we reported before (**Figure 1b, Figure S2**; for details, see Supporting Information).[14]

Genetically engineered spider silk, in conjugation to large-scale "green" fabrication, can not only offer the tunable electronic performance, but also exhibit the biocompatible and stable mechanical properties.

It is worth noting that with different polarization directions, PVDF can enhance or degrade the performance of TPNG as reported.[10] Here, the surface-potential coupling effect was simulated using COMSOL software to elucidate the electrical variation with different polarized directions of PVDF (**Figure S3**). Results show that the accordant direction of PVDF would bring about two-fold greater potentials than the opposite direction. **Figure 1c** presents a molecular model to explain the process when changing the polarization direction of PVDF. If the entire polarized direction of the PVDF layer is opposite to the electron-loss direction, where the fluorine atoms point to the PET layer, the negative potential in the PVDF layer would block the transfer of most of the electrons from spider silk to PET; by contrast, in the accordant state (hydrogen atoms point to PET), the positive PET potential generated by PVDF would attract more electrons during triboelectrification with spider silk. Furthermore, the surface potential of different polarized PVDF decorated PET is determined using Kelvin probe force microscopy (FKPM) (**Figure S4**, Supporting Information). KPFM results substantiate that the accordant direction of PVDF will increase the surface potential and strengthen the electron transferring process; meanwhile, the opposite direction of PVDF will decrease the surface potential which leads to the limit electron transferring.

The voltages generated by devices were consistent with the results above. In the pure piezoelectric-based generator (only PVDF/PET), a voltage of around 6 V was detected across a 10 MΩ resistance in series. As for the pure triboelectric-based generator (only spider silk/PET), a voltage of about 95 V was measured. While in the accordant state of matching, the voltage increased to 208 V, which was about twice the value produced by the pure triboelectric generator. Next, we applied a high electric field to reverse the polarization of phase-separated PVDF to verify the above simulation (**Figure S5**). If piezoelectric and triboelectric directions were matched on the opposite side, the voltage decreased to ~40 V, which was around the half of the original voltage produced by the triboelectric generator. In general, algebraic addition of the voltages generated by TENG and PENG cannot explain the performance we achieved. As we believed, the voltage output can be derived from piezoelectric and triboelectric synergetic work. In detail, the piezoelectric process is a dynamic process, which is related to time and applied force. The timely change of piezoelectric voltage also causes the variation of material property in self-matched PET layer. In general, the eventual voltage output of TPNG can be the nonlinear superposition of voltage generated by TENG and PENG (details see Supporting Information). And TENG and PENG operated separately without the relevant electric-field influence cannot explain the improved energy output in our system.[6-10]

To further investigate the self-matching approach, we tested piezoelectric modulation between two identical materials (**Figure S6**). Interestingly, the same

tendency could happen on the PET-PET based TENG. Normally, TENG using the same material as paired layers cannot generate significant triboelectric output because of the identical electron work function in both layers (same surface potential) and similar curvature-induced energy shifts in the surface states.[12] However, if we matched the PVDF with PET in different polarized directions to induce an opposite electron potential, a conspicuous output voltage of 41 V could be detected, suggesting that PVDF could change the PET surface electron states effectively. These results not only illustrate the contribution of self-matched PET/PVDF to the output performance of our TPNG, but also uncover the intrinsic mechanism of enhancement in hybrid TPNG components, thus laying a foundation for the development of highly efficient energy harvesters in the future.

Since PVDF is essential for the function of the PET layer, it is useful to enhance the polarization intensity of PVDF. PVDF is a semi-crystalline polymer with three main crystalline phases: a trans-gauche-trans-gauche (TGTG') α-phase; an all trans (TTT) planar zigzag β-phase; and a T_3GT_3G' γ-phase.[25] Among these phases, the β/γ-phases produce the piezoelectric performance. Therefore, a higher content of piezoelectric phases produces the optimum functioning PET layer (**Figure 2a**). Since it was reported previously that PVDF membranes fabricated through natural evaporation from DMF usually exhibited unsatisfying performance,[26] we exploited vapor-induced phase-separation process to fabricate highly polarized piezo-PVDF. Besides, graphene, with the large negative π-electron cloud which could work with the $-CH_2-$ groups in the PVDF chains, can be applied as the dopants

to help increase the piezoelectric phase in PVDF.[18,27] To investigate the superiority of vapor-induced phase-separation process and graphene, we employed Fourier Transform Infrared Spectrum (FT-IR) analysis to characterize the β/γ-phase of raw PVDF (black curve), natural-evaporated PVDF membrane (red curve), phase-separated PVDF without (blue curve) and with graphene doping (pink curve), as shown in **Figure 2b(i)**. Because different phases have distinct conformations, their infrared spectra are different and can be utilized to distinguish the conformation of samples.[28] In **Figure 2b(i)**, unprocessed raw PVDF exhibits α-phase predominantly; and, the natural-evaporated PVDF membrane still exhibits some α-phase but the amount of β/γ-phase increases. However, the near disappearance of α-phase bands demonstrates the effective polarization of most PVDF chains obtained from the phase-separation process. Moreover, the β/γ-phase content can be further increased by introducing graphene. (Supporting Information and **Figure S7**). These samples were also examined with small-angle X-ray diffraction (XRD) analyses as presented in **Figure 2b(ii)**. The characteristic diffraction peaks of original α-PVDF at 2θ of 17.7°, 18.2°, 19.9° and 26.4° are all disappeared and the appearance of new peaks at $2\theta \approx 18.6°$ of γ (110) and 20.6° of β (200/110) indicates the formation of piezo-phase PVDF.[28] Also, graphene promoted an increase in the area of diffraction peak at $2\theta \approx 20.6°$, demonstrating a potent role of graphene, in consistent with the FT-IR analysis. The amount of doped graphene may reduce the crystalline piezo-phase content of PVDF. In order to optimize the performance of PVDF, a series of phase-separated PVDF samples with

different graphene contents were fabricated for XRD testing. The amount of different crystalline phases can be obtained by deconvolution of the XRD results (details see **Figure S8** and Supporting Information). As shown in **Figure 2c**, when the graphene content was increased to 0.25 wt.%, the crystalline β-phase content reached the highest of 82% while crystalline α-phase content decreased to 4-5%. At the same time, the increment of α-phase in PVDF after over 0.25 wt.% addition of graphene may be caused by the blocking effect of graphene. Compared with graphene, the polarized effect created by water is much greater. Therefore, if water was blocked by graphene, the α-phase content would still increase even under higher graphene contents.[18] In general, the synergetic work of graphene and water in vapor induced the high content of piezo-phases in PVDF (the insert in Figure 2c). Based on the 0.25 wt.% graphene content, graphene sheets can cooperate with water molecular, providing optimum performance of PVDF.

During the vapor-induced phase-separation processing, initially transparent PVDF/graphene films became white, indicating the formation of microstructures (**Figure S9**). We examined these microstructures employing Scanning Electron Microscopy (SEM) and four major kinds of structures were found as shown in **Figure 2d**: I-nodular, II-bi-phase, III-cellular and IV-dense PVDF. Structures I-III show a porous structure while the dense morphology in structure IV shows poreless balls. The formation of these morphologies can be correlated to the compositional trajectories of the ternary phase diagram (PVDF/DMF/water) as shown in **Figure 2e**.[29-31] Since the uptake of water from vapor is the major process of the phase-

separation, the changing component during this process, which is dependent on temperature (T) and relative humidity (RH), can create four major curves as marked in phase-diagram (**Figure 2e**). These routines will eventually contribute to the morphological discrepancy and bring the various porosities (see **Supporting Information** for details). As reported previously, higher porosity of PVDF membranes brings higher compressibility compared with dense membrane, which leads to the larger deformation at the identical pressure, resulting in greater mechanical energy transformation.[32,33] As shown in **Figure 2f**, the nodular I structure with 75% porosity generated higher voltage output than the dense, bi-phasic and cellular structures (**Figure S10**). These results indicate that the vapor-induced phase-separation and graphene doping make PVDF exhibit the best performance as the matching layer.

After optimizing the matching layer of PVDF/graphene and integrating this layer with spider silk, we evaluated the electrical properties of self-matched TPNG. The size of test area was 6.25 cm^2 and a motor was used to apply mechanical impulses to the device. The effective output power of TPNG was determined by monitoring the voltage and current with loading resistances ranging from 1 to 100 MΩ. Output voltage increased in a non-linear manner with load resistance while the current decreased due to the ohmic loss (**Figure 3a**).[34] Output power varied in a biphasic trend with load resistance (**Figure 3b**). Owing to the enhancement by the accordant effect, the highest output open-circuit voltage (V_{oc}) generated was ≈ 300 V, and the highest output short circuit current (I_{sc}) reached ≈ 72 μA

(device area = 6.25 cm^2, **Figure S11**). The voltage under a load resistance of ≈ 8 MΩ approached ≈ 200 V and current reached ~12 μA; under these conditions the largest instantaneous power was ≈ 2.51 mW corresponding to a maximum power density value of 4016 mW m^{-2}. In comparison, PVDF or its composites provide lower power density (<40 mW m^{-2}) when incorporated in PENG.[28] As shown in **Table 1**, compared with other hybrid nanogenerators in which matching was not incorporated, our hybrid TPNG provided the highest output power density. As shown in **Figure 3c**, besides the electrical performance test, the stability and durability tests over 18,000 cycles are also conducted to confirm the outstanding robustness of the self-matched TPNG.

Although advances in developing small-scale energy harvesters have been made, it will be important to scale up the fabrication of TPNG for large area applications. To this end, we built a roll-to-roll continuous fabrication prototype in the laboratory for potential mass production (**Figure 3d**). The PVDF/graphene and spider silk solutions were sprayed onto substrates using nozzles, and the PVDF/graphene was passed through a vapor/heat zone while simultaneously drying the spider silk. Without needing any complex equipment or large energy consumption, the whole fabrication process was simple, environmental-friendly and energy efficient. As shown in **Figure 3e**, A5-sized (14.8 × 21.0 cm) spider silk and PVDF/graphene integrated layers were fabricated using this method. We cut out an area of 48 cm^2 (6.0 × 8.0 cm) to demonstrate a self-matched TPNG, which could power a commercial white LED (3 W) by hand tapping (**Video S1**). Then,

we calculated the energy conversion efficiency in **Figure 3f**. The output energy density of such TPNG reached 0.56 mJ m^{-2} compared to the input energy density of 1.1 mJ m^{-2}, representing a 50.9% energy conversion efficiency. Compared with pure spider silk-based TENG, the energy conversion efficiency increased significantly under the matching of piezo-PVDF.[14] More importantly, since the spider silk and PVDF are both biocompatible, the self-matched couple would be potentially suitable for various wearable or implantable devices by replacing the ancillary compositions with more biocompatible materials or implementing biocompatible encapsulations.

Based on the high voltage output and excellent mechanical flexibility of our TPNG, a number of implantable devices can be envisioned including monitoring heart, chest, stomach and bladder signals, and sensing strains accompanying the motion of arms, hands, knees and feet as schematically illustrated in **Figure 4a**. We applied our TPNG to monitor and harvest energy from the heart beats of rats. A small-scale spider silk/PVDF-graphene based TPNG was fabricated (1.5 × 1.5 cm, **Figure S12**), sealed in silk-based packages using pervious reported methods, sterilized and then implanted in the chest of a Sprague-Dawley rat (**Figure 4b (i)**; see the Experimental Section for details).[35,36] It is worth noting that the biocompatible silk-based pocket and the flexibility of the TPNG ensure the bio-safety during implantation and extraction after predesigned lifetime. The device was then connected to a rectifier and a capacitor (4.7 μF) to collect mechanical energy (**Figure 4b (ii)**). With the beating of the heart, the TPNG was compressed

and released, thus generating current flow. The fluctuating peak current signals (**Figure 4c**) generated by the beating heart are due to uneven breathing caused by the anesthetization (**Video S2**). The inset shows that the storage voltage of a 4.7 μF capacitor connected reaches ≈ 0.5 V within 5 min. The rat remained alive after a lengthy monitoring period over 3 hours. This suggests that the TPNG could be implanted in various human tissues to monitor the movements of the stomach, chest, and bladder and indicates considerable potential for *in vivo* applications in self-powered medical monitoring and treatment.[37,38]

In addition, a set of small-scale TPNGs (1 cm × 2 cm) were attached to gloves to create a gesture detector as shown in **Figure 4d**. Five TPNGs were attached on the five fingers and numbered: little finger-1, ring finger-2, middle finger-3, index finger-4, and thumb-5. As the fingers bend, the generated pressure on each TPNG triggers an output signal. For example, the gestures of "Victory" and "OK" as shown in the digital photos of **Figure 4e**, generate different voltage signals in fingers 1 to 5. Thus, a "Victory" gesture generates high voltages fingers 1, 2, and 5 as a result of the bending of fingers 1, 2 and 5 to produce this gesture. By contrast, in an "OK" gesture, fingers 4 and 5 were bent resulting in high voltages signals in these fingers. When the fingers were bent to a larger degree, higher voltage signals were detected which can be ascribed to larger contact areas at larger bending angles. Our spider silk/PVDF-graphene based TPNG can convert mechanical energy to electrical output through an innovative self-matching process, promising potential applications in future personal health-

care and clinical medicine, such as motion monitors, heart pacemakers, etc. Furthermore, the large-scale, green and facile fabrication process can promote the practical applications of this product.

Conclusion

In summary, we have developed a "self-matched" hybrid TPNG with significantly enhanced energy output through a structural and surface-potential matching approach. Specifically, the TPNG was fabricated using a facile yet effective vapor-induced phase-separation process with graphene doping to obtain a highly polarized PVDF membrane for improving the triboelectric output of spider silk and PET. The morphology and piezo-phases content of PVDF can be readily regulated by controlling the phase-separation process and the graphene content. Efficient energy transformation and outstanding output energy performance make this biocompatible spider silk/PET/PVDF-based TPNG superior to many previously reported hybrid nanogenerators. The vapor-processed PVDF membrane, in conjugation with PET and genetically engineered spider silk, not only offers significant improvement for self-powered systems, but also further illustrates the charge-transfer mechanism in nanogenerators. For proof-of-concept, our TPNG devices have been successfully applied as a self-powered wearable gesture detector and *in vivo* cardiac monitor through direct integration with wearable and implantable sensors. Multi-level modification of materials (e.g., genetic modification, chemical

conjugation and nanomaterials doping) and multi-functional integration into intelligent systems (e.g. e-skins, artificial muscles and soft robotics) can further provide potential opportunities to approach the "green" and the human-friendly intelligent IoTs era.

Experimental Section

Materials: Sodium chloride (NaCl, AR, Sigma), magnesium chloride ($MgCl_2$, AR, Sigma), PVDF powder (molecular weight: 107 000, Sigma), N, N-dimethylformamide (DMF, AR, Sigma) were purchased and used as is without further purification. Graphene was purchased from Shanghai Xiwang Technology Co., Ltd. (Shanghai, China).

Vapor-induced Phase-separation Preparation: PVDF was dissolved into DMF (10 wt.%) at 60 °C with stirring. Specific amount of graphene was added into solutions and stirred in 1 hour for fully dispersion. The obtained solution was dipped onto 2-3 mL PET substrates and then put into a spin-coater (KW-4B, Setcas, China) with speed of 1000 rmp min^{-1} in 10 seconds. A culture dish containing water or aqueous solution of salt was placed under a glass slide in a transparent sealed container. The relative humidity (RH) of <20% was obtained through re-locating to an air-drying oven directly, without any water or aqueous solution source. The RH of 20%~40% was established by using the supersaturation solution of $MgCl_2$. The RH of

>40% was maintained through the supersaturation solution of NaCl. And the temperature was controlled by an electric heater beneath.

Recombinant Spider Silk Protein Preparation: Recombinant plasmids expressing various repetitive units of dragline silk-like protein MaSp1 were constructed as previously. The recombinant spider silk proteins were expressed and purified according to the previously reported protocols.[39] Briefly, E. coli BL21(DE3) cells harboring the silk expression plasmid were treated with isopropyl-β-D-thiogalactopyranoside at 1 × 10^{-3} M for ≈ 6 h to induce silk expression. The induced cells were then harvested and resuspended in a binding buffer (10 × 10^{-3} M Tris-HCl, 150 × 10^{-3} M sodium chloride, 5 × 10^{-3} M imidazole, pH 8.0). After sonication to disrupt the cells, the mixture was centrifuged at 9000 g for 20 min at 20 ℃ and the supernatant was loaded onto a column with pre-charged Ni-NTA Sepharose beads pre- equilibrated with the binding buffer. The column was washed with buffer A (10 × 10^{-3} M Tris-HCl, 150 × 10^{-3} M sodium chloride, 60 × 10^{-3} M imidazole, pH 8.0) and eluted with buffer B (10 × 10^{-3} M Tris-HCl, 50 × 10^{-3} M sodium chloride, 150 × 10^{-3} M imidazole, pH 8.0). The eluted protein was dialyzed for 2 d against distilled water using Slide-a-Lyzer dialysis cassettes (MWCO 3500, Pierce, USA). The purity of protein samples was determined by sodium dodecyl sulfate polyacrylamide gel electrophoresis. Finally, the spider silk solution was frozen at -80 ℃ for 12 h and lyophilized until complete sublimation of water.

Fabrication of the TPNG: Firstly, the lyophilized spider silk was dissolved in water at 5 mg mL^{-1}. Then the solution was placed at 4 ℃ for 6 h and filtered with 2.5 μm membrane to eliminate insoluble particles. The PET/ITO substrate (thickness: 175 μm, resistance: 5-7 Ω m^{-2}) was previously treated with 5-min oxygen plasma for better hydrophilicity. Then, the spider silk solution was printed on the PET/ITO substrate using a commercial inkjet printer (Dimatix DMP 2800 equipped with Dimatix Materials Cartridges, Fujifilm, Santa Clara, CA, USA). For details, see Figure S10 and Supporting Information. After dried in an oven at 60 ° C for 10 min, the as-prepared Spider silk/PET/ITO was assembled with another PET/PVDF-graphene/Cu layer, to obtain the final TPNG. To fabricate the implantable TPNG, two layers of the TPNG are fixed together with a 100-μm-thick silk-based spacer set between them, and two lead wires are connected respectively to the electrodes. After assembling into an arch-shape structure, the whole device is encapsulated in a silk-based “pocket”. Silk encapsulation layers are fabricated by the casting and water-annealing method and cut into a proper size. The as-fabricated TPNG is set between two silk encapsulation layers. Then, silk solution (degummed for 30min) is used as an adhesive to carefully stick the edge of the two encapsulation layers. The device is air-dried for 12 hours in a sterilized UV chamber to exclude any interstice and ensure that the TPNG is protected from the physiological environment.

Animal Experiments: Sprague-Dawley rats were purchased from SLAC Laboratory Animal (Shanghai). All the rats are male with an average weight of 120 g, fed in the Department of Laboratory Animal Science for 5 d before experiments. All animal studies were approved by the Institutional Animal Care and Use Committee of Fudan University. Rats were anesthetized by intraperitoneally injecting a ketamine/xylazine mix and then placed in a sealed chamber with 5% isoflurane. Depth of anesthesia was monitored by palpebral and withdrawal reflexes to confirm that the animal had reached "stage 3" of anesthesia. Once the animal was lightly anesthetized, the chest was shaved and cleaned the incision site with 70% ethanol, followed by a betadine surgical scrub. Once stage 3 was confirmed, a small longitudinal incision was made at the chest region of the anesthetized mouse. After layer-by-layer opening operation, the sterile implant (flexible sealed TPNG) was conformable placed on the thorax wall directly above the heart. The incision was closed with a Dexon 5-0 suture. The animal was monitored under the anesthesia station.

Characterization and measurement: KPFM measurements were carried out using the tapping mode (AFM, CYPHER ES) with a conductive noncontact cantilever coated with Pt. The morphology of the PVDF film was observed by SEM (SEM, TESCAN MIRA3) at an accelerating voltage of 5 kV. Fourier transform infrared spectroscopy (FT-IR) was performed using a Bruker Vertex 70v FT-IR spectrometer. Small angle X-ray diffraction (XRD) patterns were obtained from an X-ray diffractometer (Bruker D8 ADVANCE) with a monochromatic source of Cu Kα1 radiation (λ = 0.15405 nm) at 1.6

kW (40 kV, 40 mA). A liner motor was applied as the external force (operating distance, 1 cm). In addition, the output voltage and current of the TPNG were measured using a digital oscilloscope (HMO3002 Series, Rohde & Schwarz) and a semiconductor parameter analyzer (Keithley 4200-SCS, Tektronix), respectively.

Supporting Information

Supporting Information is available from the Wiley Online Library or from the author.

Acknowledgements

T.H. and Y.Z. contributed equally to this work. This work was partially supported by the National Science and Technology Major Project from Minister of Science and Technology, China (Grant No. 2018AAA0103100), the National Science Fund for Excellent Young Scholars (Grant No. 61822406), the National Natural Science Foundation of China (Grant No. 51802337, 11774368, 11804353, and 61574156), Shanghai Outstanding Academic Leaders Plan (Grant No. 18XD1404700). The authors thank Shiduo Cheng and Prof. Xianying Wang (University of Shanghai for Science and Technology) for the assistance in KPFM measurements.

Received:

Revised:

Published online:

References

[1] W. Gao, S. Emaminejad, H. Yin, Y. Nyein, S. Challa, K. Chen, A. Peck, H. M. Fahad, H. Ota, H. Shiraki, D. Kiriya, D. Lien, G. A. Brooks, *Nature* **2016**, *529*, 509.

[2] M. Bariya, H. Yin, Y. Nyein, A. Javey, *Nat. Electron.* **2018**, *1*, 167.

[3] X. Pu, H. Guo, J. Chen, X. Wang, Y. Xi, C. Hu, Z. L. Wang, *Sci. Adv.* **2017**, *3*, 1700694.

[4] S. B. Jeon, S. J. Park, W. G. Kim, I. W. Tcho, I. K. Jin, J. K. Han, D. Kim, Y. K. Choi, *Nano Energy* **2018**, *53*, 596.

[5] X. Cao, Y. Jie, N. Wang, Z. L. Wang, *Adv. Energy Mater.* **2016**, *6*, 1600665.

[6] B. Shi, Q. Zheng, W. Jiang, L. Yan, X. Wang, H. Liu, Y. Yao, Z. Li, Z. L. Wang, *Adv. Mater.* **2016**, *28*, 846.

[7] Q. Zheng, B. Shi, Z. Li, Z. L. Wang, *Adv. Sci.* **2017**, *4*, 1700029.

[8] C. Zhao, Q. Zhang, W. Zhang, X. Du, Y. Zhang, S. Gong, K. Ren, Q. Sun, Z. L. Wang, *Nano Energy* **2019**, *57*, 440.

[9] S. Chen, X. Tao, W. Zeng, B. Yang, S. Shang, *Adv. Energy Mater.* **2017**, *7*, 1601569.

[10] Y. Guo, X. S. Zhang, Y. Wang, W. Gong, Q. Zhang, H. Wang, J. Brugger, *Nano Energy* **2018**, *48*, 152.

[11] C. Xu, Y. Zi, A. C. Wang, H. Zou, Y. Dai, X. He, P. Wang, Y. Wang, P. Feng, D. Li, Z. L. Wang, *Adv. Mater.* **2018**, *30*, 1706790.

[12] C. Xu, B. Zhang, A. C. Wang, H. Zou, G. Liu, W. Ding, *ACS Nano* **2019**, *13*, 2034.

[13] Z. L. Wang, *ACS Nano* **2013**, *7*, 9533.

[14] Y. Zhang, Z. Zhou, L. Sun, Z. Liu, X. Xia, T. H. Tao, *Adv. Mater.* **2018**, *30*, 1805722.

[15] S. Shin, Y. H. Kwon, Y. Kim, J. Jung, M. H. Lee, *ACS Nano* **2015**, *9*, 4621.

[16] H. Y. Li, L. Su, S. Y. Kuang, C. F. Pan, G. Zhu, Z. L. Wang, *Adv. Funct. Mater.* **2015**, *25*, 5691.

[17] F. R. Fan, W. Tang, Z. L. Wang, *Adv. Mater.* **2016**, *28*, 4283.

[18] T. Huang, S. Yang, P. He, J. Sun, S. Zhang, D. Li, Y. Meng, J. Zhou, H. Tang, J. Liang, G. Ding, X. Xie, *ACS Appl. Mater. Interfaces* **2018**, *10*, 30732.

[19] X. Chen, X. Han, Q. D. Shen, *Adv. Electron. Mater.* **2017**, *3*, 1600460.

[20] Y. H. Jung, S. K. Hong, H. S. Wang, J. H. Han, T. X. Pham, H. Park, J. Kim, S. Kang, C. D. Yoo, K. J. Lee, *Adv. Mater.* **2019**, DOI:10.1002/adma.201904020.

[21] H. Zhu, S. Yamamoto, J. Matsui, T. Miyashita, M. Mitsuishi, *J. Mater. Chem. C* **2014**, *2*, 6727.

[22] X. Liu, J. Ma, X. Wu, L. Lin, X. Wang, *ACS Nano* **2017**, *11*, 1901.

[23] N. A. Hoque, P. Thakur, S. Roy, A. Kool, B. Bagchi, P. Biswas, M. Saikh, F. Khatun, S. Das, P. P. Ray, *ACS Appl. Mater. Interfaces* **2017**, *9*, 23048.

[24] C. A. Mizzi, A. Y. W. Lin, L. D. Marks, *Phys. Rev. Lett.* **2019**, *123*, 116103.

[25] P. Martins, A. C. Lopes, S. Lanceros-Mendez, *Prog. Polym. Sci.* **2014**, *39*, 683.

[26] P. Xiao, N. Yi, T. Zhang, Y. Huang, H. Chang, Y. Yang, Y. Zhou, Y. Chen, *Adv. Sci.* **2015**, *3*, 1500438.

[27] S. K. Karan, R. Bera, S. Paria, A. K. Das, S. Maiti, A. Maitra, B. B. Khatua, *Adv. Energy Mater.* **2016**, *6*, 1601016.

[28] Y. Bormashenko, R. Pogreb, O. Stanevsky, E. Bormashenko, *Polym. Test* **2004**, *23*, 791.

[29] M. Li, I. Katsouras, C. Piliego, G. Glasser, I. Lieberwirth, P. W. M. Blom, D. M. De Leeuw, *J. Mater. Chem. C* **2013**, *1*, 7695.

[30] T. Huang, P. He, R. Wang, S. Yang, J. Sun, X. Xie, G. Ding, *Adv. Funct. Mater.* **2019**, *29*, 1903732.

[31] A. Venault, Y. Chang, D. M. Wang, D. Bouyer, *Polym. Rev.* **2013**, *53*, 568.

[32] Z. Zhang, C. Yao, Y. Yu, Z. Hong, M. Zhi, X. Wang, *Adv. Funct. Mater.* **2016**, *26*, 6760.

[33] Y. Mao, P. Zhao, G. McConohy, H. Yang, Y. Tong, X. Wang, *Adv. Energy Mater.* **2014**, *4*, 1301624.

[34] Y. Zi, S. Niu, J. Wang, Z. Wen, W. Tang, Z. L. Wang, *Nat. Commun.* **2015**, *6*, 8376.

[35] W. Jiang, H. Li, Z. Liu, Z. Li, J. Tian, B. Shi, Y. Zou, H. Ouyang, C. Zhao, L. Zhao, R. Sun, H. Zheng, Y. Fan, Z. L. Wang, Z. Li, *Adv. Mater.* **2018**, *30*, 1801895.

[36] Y. Zhang, Z. Zhou, Z. Fan, S. Zhang, F. Zheng, K. Liu, Y. Zhang, Z. Shi, L. Chen, X. Li, Y. Mao, F. Wang, Y. L. Sun, T. H. Tao, *Small* **2018**, *14*, 1802050.

[37] C. Li, J. Adamcik, R. Mezzenga, *Nat. Nanotechnol.* **2012**, *7*, 421.

[38] Q. Zheng, Y. Zou, Y. Zhang, Z. Liu, B. Shi, X. Wang, Y. Jin, H. Ouyang, Z. Li, Z. L. Wang, *Sci. Adv.* **2016**, *2*, 1501478.

[39] X. Xia, Z. Qian, C. Seok, Y. Hwan, D. L. Kaplan, S. Yup, *Proc. Natl. Acad. Sci.* **2010**, *107*, 14059.

[40] V. Bhavanasi, D. Y. Kusuma, P. S. Lee, *Adv. Energy Mater.* **2014**, *4*, 1400723.

[41] J. Sun, X. Pu, M. Liu, A. Yu, C. Du, J. Zhai, W. Hu, Z. L. Wang, *ACS Nano* **2018**, *12*, 6147.

[42] Q. Zheng, L. Fang, H. Guo, K. Yang, Z. Cai, M. A. B. Meador, S. Gong, *Adv. Funct. Mater.* **2018**, *28*, 1706365.

[43] S. Paria, R. Bera, S. K. Karan, A. Maitra, A. K. Das, S. K. Si, L. Halder, A. Bera, B. B. Khatua, *ACS Appl. Energy Mater.* **2018**, *1*, 4963.

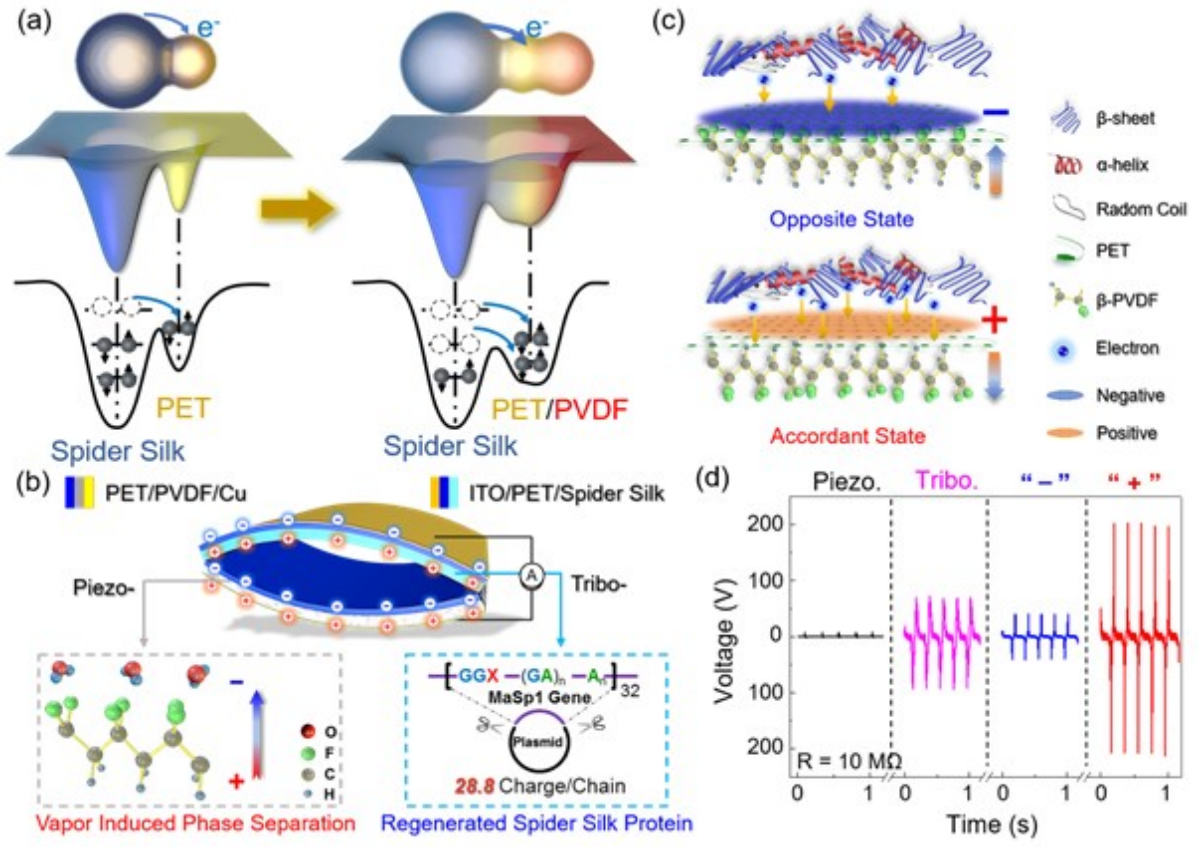

Figure 1. Design of TPNG using the self-matching approach. a) An electron-cloud-potential-well model proposed to explain the charge transfer between spider silk and PET with/without PVDF (arrows indicate electron transfer events). b) A schematic model of a TPNG model composed of vapor-induced phase-separated PVDF (grey dashed box) and regenerated spider silk protein (blue dashed box). c) Molecular models to illustrate the electron transferring state of the opposite (Tribo "−" Piezo) and accordant (Tribo "+" Piezo) states. d) The voltage signals generated by pure PENG (only PVDF/PET), TENG (only spider silk/PET), Tribo "−" Piezo, and Tribo "+" Piezo with R=10 MΩ in series.

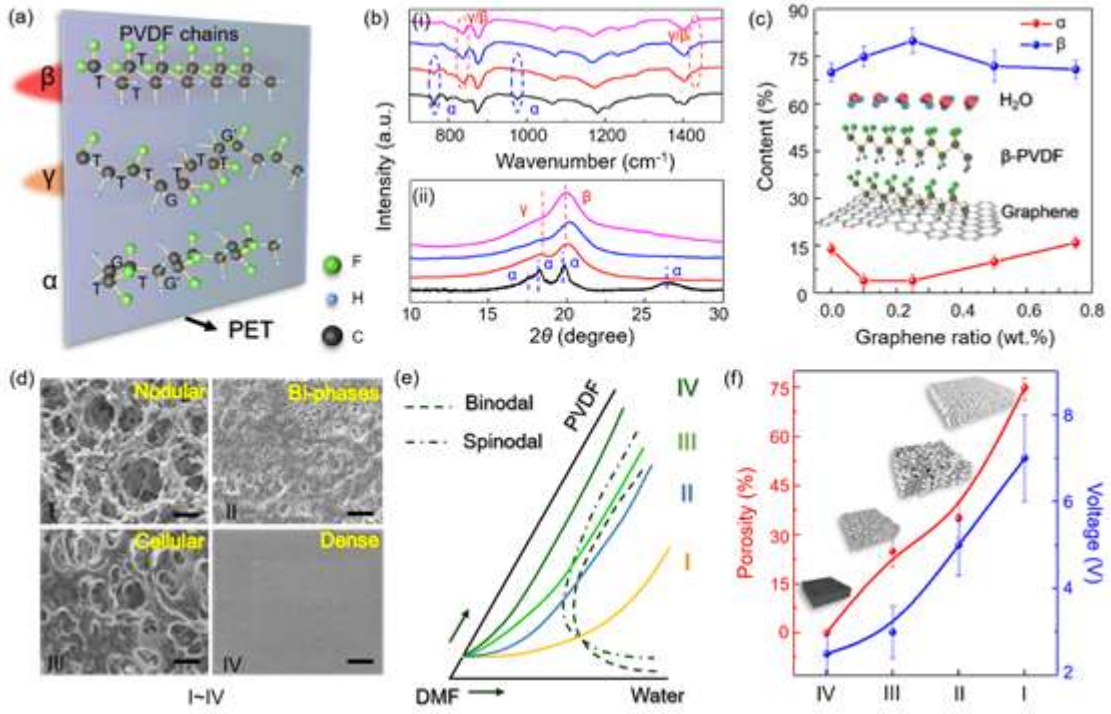

Figure 2. Tuning of matched piezo-PVDF by optimizing piezoelectric phases, doping content, and surface morphologies. a) A 3D model for illustrating the different configurations of PVDF and their effect on surface-potential differences of PET. (The depth of the color corresponding to the modified intensity of the PET) b) The (i) FT-IR spectra and (ii) XRD results for: raw powder (black curve), natural-evaporated PVDF membranes (red curve), phase-separated PVDF film without (blue curve), and with graphene doping (pink curve). c) Deconvolution analyses of the XRD results showing α and β phase contents with different ratios of graphene doping. d) SEM images of the different morphologies observed in phase-separated PVDF films (I: nodular; II: bi-phases; III: cellular; IV: dense structures, scale bar, 2 μm). e) Schematic isothermal ternary phase diagram of PVDF/DMF/H_2O without a specific concentration scale. f) The porosity of I-IV structures and associated voltage signals.

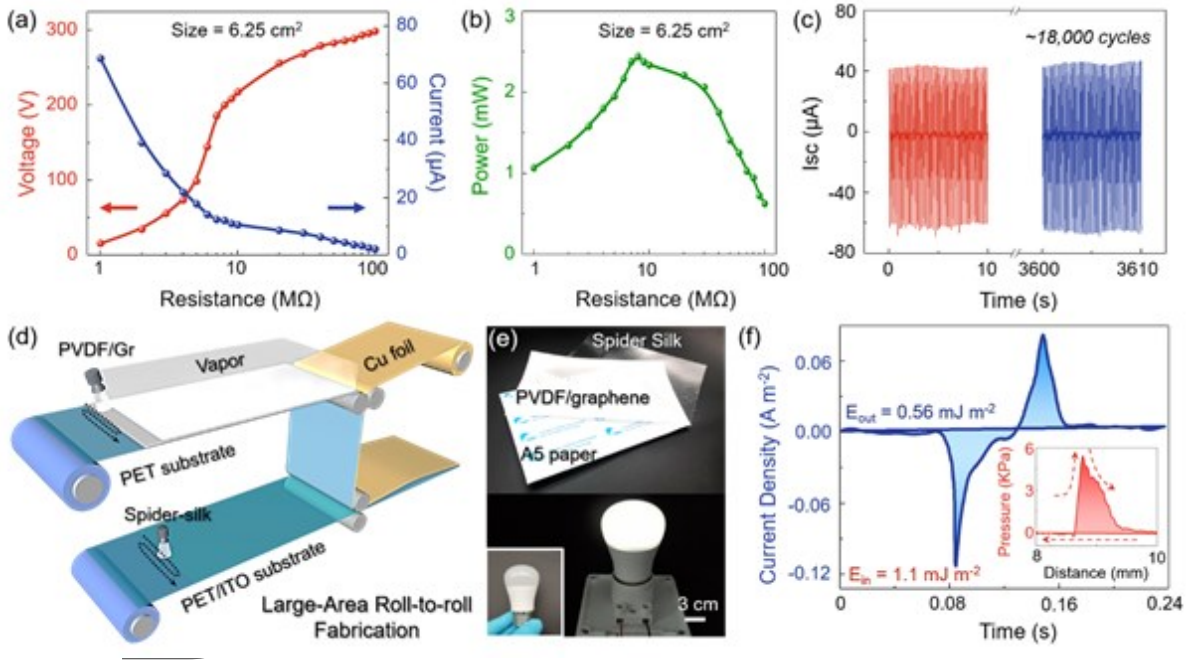

Figure 3. Spider silk/PET/PVDF based TPNG performance. a) Dependence of output voltage and current on external load resistance. b) Dependence of output power on external load resistance. c) I_{sc} measured over ~18,000 cycles. d) Schematic for large-scale and continuous fabrication of TPNG. e) Digital photos of A5-size phase-separated PVDF and spider silk films and the white LED light (3 W) lightened by a 48-cm^2 TPNG, the insert shows the LED light without powering. f) The output current density of one cycle. The inset shows input pressure created by hand-tapping as a function of distance.

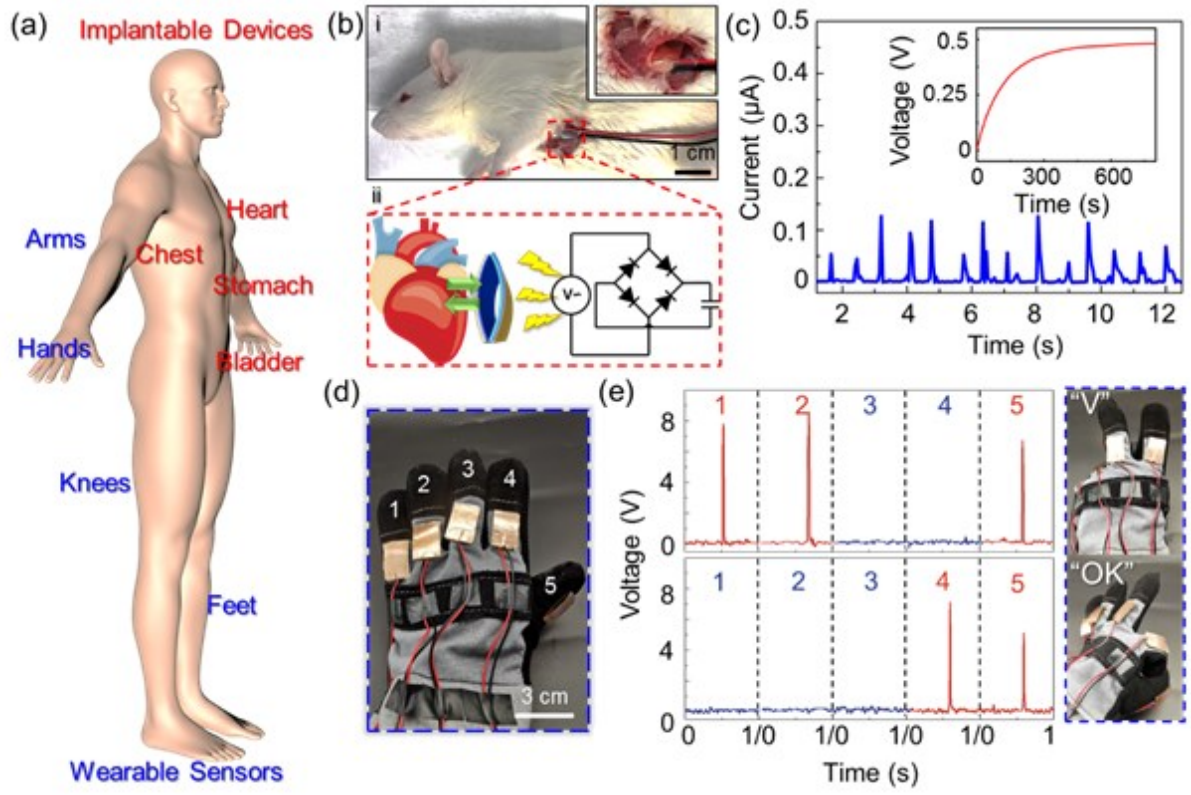

Figure 4. Demonstration of TPNGs as implantable organ monitors, bio-energy harvesters and wearable hand-gesture sensors. a) Schematic illustration of the numerous applications of TPNG in wearable sensors and implantable devices. b) (i) Images of an TPNG located in the subdermal chest region at two different scales; (ii) Schematic of the energy harvesting process and circuit as applied to collect energy from a beating rat heart. c) Current signals of implanted TPNG associated with the beating heart; inset shows the voltage developed across a capacitor storing charge from accumulated current signals from the beating heart. d) Photograph of TPNG-based gesture monitoring glove. e) Recorded voltage signals on the five fingers when making "Victory" and "OK" gestures.

Table 1. Comparison of various TENG, PENG, and TPNGs.

Materials	Type	Device Area [cm^2]	**Power Density [$mW\ m^{-2}$]**	Voc [V]	Isc [μA]
PVDF-TrFE nanotubes[40]	Piezo.	0.78	**22**	4.8	N/A
AlO-rGO/PVDF[28]	Piezo.	7.8	**36**	36	0.8
PDMS (self-healing)[41]	Tribo.	6	**327**	94	1
Spider Silk[14]	Tribo.	6	**1030**	145	17
Porous PDMS[42]	Tribo.	2	**2330**	60	7.7
$BaTiO_3$/PDMS[6]	Tribo.+Piezo.	2.25	**97.41**	60	1
PVDF+Silk (nanowire)[10]	Tribo.+Piezo.	8	**3100**	500	12
PVDF+Paper[43]	Tribo.+Piezo.	15	**3700**	342	8.1
Spider Silk/PET/PVDF	Tribo.+Piezo.	6.25	**4016**	300	72

Keyword tribo-/piezoelectric nanogenerator, spider silk, vapor-induced phase-separation, implantable energy harvester

Tao Huang[†], Yujia Zhang[†], Peng He, Gang Wang, Xiaoxia Xia, Guqiao Ding[*] and Tiger H. Tao[*]

"Self-matched" Tribo-/Piezoelectric Nanogenerators Using Vapor-induced Phase-separated Polyvinylidene Fluoride and Recombinant Spider Silk

Self-matched tribo-/piezo-nanogenerator (TPNG), composed of genetically engineered recombinant spider silk protein and piezoelectric polyvinylidene fluoride (PVDF)-decorated polyethylene terephthalate (PET) layer, generates a greatly enhanced energy output. As the structural and electron-potential match, the power density from TPNG can reach 4016 mW m^{-2} and energy transform efficiency is 50.9%, suggesting potential applications in implantable and wearable electronics.

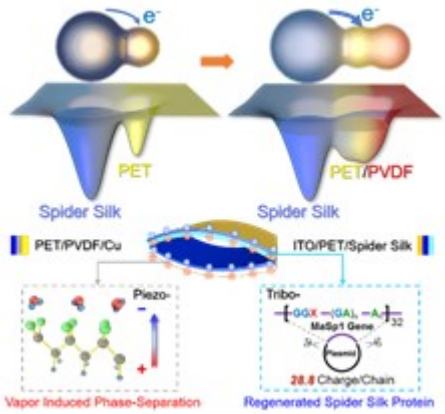

Author/s:
Huang, T;Zhang, Y;He, P;Wang, G;Xia, X;Ding, G;Tao, TH

Title:
"Self-Matched" Tribo/Piezoelectric Nanogenerators Using Vapor-Induced Phase-Separated Poly(vinylidene fluoride) and Recombinant Spider Silk.

Date:
2020-03

Citation:
Huang, T., Zhang, Y., He, P., Wang, G., Xia, X., Ding, G. & Tao, T. H. (2020). "Self-Matched" Tribo/Piezoelectric Nanogenerators Using Vapor-Induced Phase-Separated Poly(vinylidene fluoride) and Recombinant Spider Silk.. Adv Mater, 32 (10), pp.e1907336-. https://doi.org/10.1002/adma.201907336.